Exact stationary solutions of the parametrically driven and damped nonlinear Dirac equation

Cite as: Chaos **29**, 093129 (2019); doi: 10.1063/1.5115505
Submitted: 18 June 2019 · Accepted: 6 September 2019 ·
Published Online: 30 September 2019

Niurka R. Quintero[a] and Bernardo Sánchez-Rey[b]

AFFILIATIONS

Física Aplicada I, Escuela Politécnica Superior, Universidad de Sevilla, Virgen de África 7, 41011, Sevilla, Spain

[a]**Electronic mail:** niurka@us.es. **Also at:** Física Aplicada I, Escuela Técnica Superior de Ingeniería Informática, Universidad de Sevilla, Avda Reina Mercedes s/n, 41012 Sevilla, Spain.
[b]**Electronic mail:** bernardo@us.es

ABSTRACT

Two exact stationary soliton solutions are found in the parametrically driven and damped nonlinear Dirac equation. The parametric force considered is a complex ac force. The solutions appear when their frequencies are locked to half the frequency of the parametric force, and their phases satisfy certain conditions depending on the force amplitude and on the damping coefficient. Explicit expressions for the charge, the energy, and the momentum of these solutions are provided. Their stability is studied via a variational method using an ansatz with only two collective coordinates. Numerical simulations confirm that one of the solutions is stable, while the other is an unstable saddle point. Consequently, the stabilization of damped Dirac solitons can be achieved via time-periodic parametric excitations.

The stabilization of damped nonlinear Dirac solitons is addressed by considering a time-periodic parametric force that supplies the required balance between energy losses and gains. A remarkable finding is that we specifically obtain two exact stationary soliton solutions and derive the sufficient conditions for their existence. Their stability is studied by using a variational approach with only two degrees of freedom, which reduces the original problem to an autonomous dynamical system with two fixed points corresponding to the two stationary solutions. It is shown that one of these solutions is stable, whereas the other is unstable. In addition to a stability diagram in the parameter space, we analyze phase portraits that provide a global and detailed view of the dynamics around the stationary solutions. These predictions are fully confirmed by numerical simulations of the parametrically driven, damped NLD equation.

I. INTRODUCTION

The study of parametric forces has attracted the attention of theorists and experimentalists in recent years.[1–4] Parametric pumping is identified with a driving acting on the system, which is modeled through time modulation of a system parameter. Diverse responses of systems under parametric driving have been observed, such as the formation of Faraday waves in Bose-Einstein condensates,[5,6] the convective motion of vibrated granular media,[7] the unidirectional motion of kinks in the sine-Gordon equation[8] and of microdrops on a plate surface,[9] the control of the shape of a ribbon formed from paramagnetic colloids,[10] and the suppression of chaos of a single-mode laser with modulated losses.[11] Furthermore, parametric pumping has been used to compensate the dissipative effect in soliton theory,[12,13] to induce an anomalous resonance phenomenon in ϕ^4 models[14] and to stabilize damped nonlinear Schrödinger solitary waves.[15,16]

In particle systems, a time-periodic function is usually employed as a parametric force.[17–19] In extended systems, soliton dynamics has been studied not only under the influence of time-periodic parametric forces, but also under spatially periodic forces.[20–26] In the latter case, a length scale competition arises between the spatial period of the force and the soliton width. This characteristic phenomenon originates or enhances instabilities of the nonlinear waves.[21,24,27]

Time-periodic parametric driving of amplitude r and frequency ν has been considered in the nonintegrable, damped Φ^4 model

$$\Phi_{tt} - \Phi_{xx} - \Phi + \Phi^3 = -\rho\Phi_t + r\cos(\nu t)\Phi, \tag{1}$$

with constant dissipation coefficient ρ. In this system, the parametric force acts directly on the kink width, which causes an oscillatory

motion, and an anomalous resonance appears when ν is closed to the internal mode frequency.[14] Moreover, the formation of the so-called wobbling kink, that is, a kink with an excited internal mode, has recently been reviewed by Barashenkov (see the pedagogical review[4] and references therein). This wobbling kink can be sustained indefinitely when ν is locked to the internal mode frequency.[28,29]

The integrability of the sine-Gordon equation allows the existence of wobbling kinks in the sine-Gordon system as exact 3-soliton solutions.[30] When damping and a parametric force are introduced in the sine-Gordon model,

$$\Phi_{tt} - \Phi_{xx} + \sin\Phi = -\rho\Phi_t + r\cos(\nu t)\sin\Phi, \tag{2}$$

the translational mode is excited and, as a consequence, π-kinks propagate.[31] This last system has been derived from the Landau-Lifshitz equation, which describes the magnetization dynamics of ferromagnetic materials.[16] In this regard, $\Phi(x,t)$ represents the azimuthal angle of the unit vector of magnetization $\vec{m}$. Interestingly, for a linear combination of the y and z components of $\vec{m}$, $\psi(x,t)$, the parametrically driven and damped nonlinear Schrödinger equation has also been derived,

$$i\psi_t + \psi_{xx} + 2|\psi|^2\psi = -i\rho\psi + r\exp(i\nu t)\psi^\star. \tag{3}$$

In contrast with the nonlinear Klein-Gordon Eqs. (1) and (2), where the topological solitary waves are robust under the influence of damping, in the nonlinear Schrödinger equation, the envelope soliton disappears when dissipation is introduced. However, the parametric force provides a stabilization of the damped nonlinear Schrödinger soliton. Remarkably, for Eq. (3), two exact solutions have been found,[15] one of which is stable and the other unstable, while in the parametrically driven Φ^4 and sine-Gordon systems, only approximated solutions have been obtained by using perturbative methods.[4]

Increasing the level of complexity, here we study the parametrically driven and damped nonlinear Dirac (NLD) equation, where the wave function has consequently become a vector field with two spinor components. For the $(1+1)$ dimensional NLD equation (one time dimension plus one space dimension), analytical solitary waves have been derived.[32] Applications of the NLD equation have been found in the context of Bose-Einstein condensates,[33] and an optical analogue of Dirac solitons in binary waveguide arrays have also been studied.[34] Additionally, rich nonlinear phenomena in the NLD equation have been investigated in the presence of potentials or external driving forces.[35–37] In particular, in Ref. 38, the response of Dirac solitons to a spatially periodic parametric force was studied. When the damping is introduced, the soliton vanishes because the spatially periodic parametric force is unable to stabilize it. The aim of this work is to show that, similar to the nonlinear Schrödinger Eq. (3), a time-periodic parametric force can stabilize the damped Dirac soliton, thereby providing the required balance between energy losses and gains. In fact, it is shown that the parametrically driven, damped NLD equation also possesses two exact soliton solutions, one of which is stable and the other unstable.

The outline of the paper is as follows. In Sec. II, the parametrically driven and damped NLD equation is introduced with a complex ac parametric force, and two exact stationary soliton solutions are found. Continuity equations for the charge, the momentum, and the energy are derived in Sec. III, and explicit expressions for the charge, the momentum, and the energy of the exact stationary solitons are also obtained. Section IV is devoted to stability analysis by using a variational method and an ansatz with only two collective coordinates. Finally, the main results and the conclusions are summarized in Sec. V.

II. EXACT STATIONARY SOLITON SOLUTIONS OF THE PARAMETRICALLY DRIVEN DAMPED NLD EQUATION

The parametrically driven, damped NLD equation has been introduced for the first time in Ref. 38. There the parametric pumping is inhomogeneous and time independent. Here, motivated by the study of Ref. 15, a time-periodic complex force $f(t)$ is considered such that the parametrically driven damped NLD equation reads

$$i\gamma^\mu\partial_\mu\Psi - m\Psi + g^2(\bar{\Psi}\Psi)\Psi = f(t)\Psi^\star - i\rho\gamma^0\Psi, \tag{4}$$

where $\Psi(x,t) = \{\Psi_1(x,t);\Psi_2(x,t)\}^T$ is a vector field with two spinor components, $\bar{\Psi} = (\Psi^\star)^T\gamma^0$ is the Dirac adjoint spinor, m is the mass of a single particle, g is the coupling constant, $f(t)$ is the time-dependent parametric force, and $\rho > 0$ is the dissipation coefficient. Moreover, the following representation for the $1+1$ dimensional Dirac Gamma matrices is considered:

$$\gamma^0 = \sigma_3 = \begin{pmatrix} 1 & 0 \\ 0 & -1 \end{pmatrix}, \quad \gamma^1 = i\sigma_2 = \begin{pmatrix} 0 & 1 \\ -1 & 0 \end{pmatrix}, \tag{5}$$

where σ_2 and σ_3 are the Pauli matrices.[35,39]

The corresponding adjoint NLD equation is given by

$$i\partial_\mu\bar{\Psi}\gamma^\mu + m\bar{\Psi} - g^2(\bar{\Psi}\Psi)\bar{\Psi} = -f^\star(t)\bar{\Psi}^\star - i\rho\bar{\Psi}\gamma^0. \tag{6}$$

This equation, together with (4), can be derived in a standard way from the Lagrangian density

$$\mathscr{L} = \left(\frac{i}{2}\right)[\bar{\Psi}\gamma^\mu\partial_\mu\Psi - \partial_\mu\bar{\Psi}\gamma^\mu\Psi] - m\bar{\Psi}\Psi + \frac{g^2}{2}(\bar{\Psi}\Psi)^2 - \frac{1}{2}f\bar{\Psi}\Psi^\star - \frac{1}{2}f^\star\bar{\Psi}^\star\Psi \tag{7}$$

and from the dissipation function

$$\mathscr{F} = -i\rho(\bar{\Psi}\gamma^0\Psi_t - \bar{\Psi}_t\gamma^0\Psi). \tag{8}$$

Indeed, by inserting (7) and (8) into

$$\partial_\mu\frac{\partial\mathscr{L}}{\partial(\partial_\mu\bar{\Psi})} - \frac{\partial\mathscr{L}}{\partial\bar{\Psi}} = \frac{\partial\mathscr{F}}{\partial(\partial_t\bar{\Psi})}, \tag{9}$$

$$\partial_\mu\frac{\partial\mathscr{L}}{\partial(\partial_\mu\Psi)} - \frac{\partial\mathscr{L}}{\partial\Psi} = \frac{\partial\mathscr{F}}{\partial(\partial_t\Psi)}, \tag{10}$$

Eqs. (4) and (6) are obtained, respectively.

The NLD equation (4) without perturbation, i.e., $f(t) = 0$ and $\rho = 0$, has stationary solutions. From these solutions a NLD moving soliton can be obtained by using the Lorentz boost.[35] This traveling wave propagates with constant velocity, constant charge, constant energy, and constant momentum.

Let us consider that the parametric force is a complex ac force

$$f(t) = re^{-i\nu t}, \tag{11}$$

where the amplitude $r > 0$, and the external frequency $\nu > 0$, are real constants. Negative values of the amplitude r can be recovered by means of the transformation $\Psi(x,t) \to e^{i\pi/2}\Psi(x,t)$ in Eq. (7).

For this choice of the parametric force, exact stationary solutions of the damped parametrically NLD Eq. (4) can be found. Indeed, stationary solutions are given by

$$\Psi(x,t) = \psi(x)e^{-i\Omega t}, \tag{12}$$

where Ω is the frequency of the oscillations of the spinor components. On inserting (11) and (12) into Eq. (4), it follows that $\psi(x)$ must satisfy

$$\Omega\gamma^0\psi + i\gamma^1\psi_x - m\psi + g^2(\bar{\psi}\psi)\psi = r\psi^\star - i\rho\gamma^0\psi, \tag{13}$$

where necessarily

$$\Omega = \frac{\nu}{2}, \tag{14}$$

so that $\psi(x)$ is a function independent of time. Therefore, the oscillations of $\Psi(x,t)$ have to be locked to the frequency of the parametric driving. This is a distinctive feature of the parametrically driven nonlinear systems.[3,16,40]

Let us now assume that

$$\psi(x) = e^{-i\Theta/2}\begin{bmatrix} A(x) \\ iB(x) \end{bmatrix}, \tag{15}$$

where $A(x)$ and $B(x)$ are real functions, and Θ is a real parameter. In order to be consistent, the above assumption requires the phase Θ to take one of only two possible values,

$$\Theta_+ = \arcsin\left(\frac{\rho}{r}\right) \tag{16}$$

or

$$\Theta_- = \pi - \arcsin\left(\frac{\rho}{r}\right), \tag{17}$$

which also implies the constraint $\rho \le r$. Under the conditions (16) and (17), $A(x)$ and $B(x)$ satisfy

$$A_x + [m + \omega_\pm]B - g^2(A^2 - B^2)B = 0, \tag{18}$$

$$B_x + [m - \omega_\pm]A - g^2(A^2 - B^2)A = 0, \tag{19}$$

where

$$\omega_\pm = \nu/2 - r\cos\Theta_\pm = \frac{\nu}{2} \mp \sqrt{r^2 - \rho^2}. \tag{20}$$

By comparing (18) and (19) with the equations found by Lee *et al.* in Ref. 32, it is straightforwardly deduced that

$$A_\pm(x) = \frac{\sqrt{2}\beta_\pm}{g}\frac{\sqrt{m+\omega_\pm}\cosh(\beta_\pm x)}{m + \omega_\pm\cosh(2\beta_\pm x)}, \tag{21}$$

$$B_\pm(x) = \frac{\sqrt{2}\beta_\pm}{g}\frac{\sqrt{m-\omega_\pm}\sinh(\beta_\pm x)}{m + \omega_\pm\cosh(2\beta_\pm x)}, \tag{22}$$

where $\beta_\pm = \sqrt{m^2 - \omega_\pm^2}$. Hence, the stationary solutions of the parametrically driven, damped NLD equation

$$\Psi_\pm(x,t) = e^{-i(\nu t + \Theta_\pm)/2}\begin{bmatrix} A_\pm(x) \\ iB_\pm(x) \end{bmatrix} \tag{23}$$

have a functional form similar to that of the NLD equation without perturbations. The parametric force introduces an extra phase factor $\exp(-i\Theta_\pm/2)$ into the solution that depends on the amplitude r and on the damping coefficient ρ, and, in the spatial part of the spinor components, replaces the frequency Ω with $\omega_\pm$, which is a function of ν, r, and ρ.

III. CHARGE, MOMENTUM, AND ENERGY OF THE EXACT STATIONARY SOLUTIONS

For the generic parametrically driven and damped NLD equation (4), continuity equations for the charge, the energy, and the momentum of a Dirac soliton can be easily derived.[37] For the charge

$$Q = \int_{-\infty}^{+\infty} dx\bar{\Psi}\gamma^0\Psi \tag{24}$$

it is obtained that

$$\frac{dQ}{dt} = -2\rho Q - i\int_{-\infty}^{+\infty} dx[f\bar{\Psi}\Psi^\star - f^\star\bar{\Psi}^\star\Psi]. \tag{25}$$

For the energy

$$E = \int_{-\infty}^{+\infty} dxT^{00}, \tag{26}$$

where the energy density reads

$$T^{00} = \frac{i}{2}(\bar{\Psi}\gamma^0\Psi_t - \bar{\Psi}_t\gamma^0\Psi) - \mathscr{L}, \tag{27}$$

the evolution equation is

$$\frac{dE}{dt} = \int_{-\infty}^{+\infty} dx\left[\mathscr{F} + \frac{1}{2}\left(f_t\bar{\Psi}\Psi^\star + f_t^\star\bar{\Psi}^\star\Psi\right)\right]. \tag{28}$$

Notice that if f is time independent then $\frac{dE}{dt} = \int_{-\infty}^{+\infty} dx\mathscr{F}$, and there is no possibility of compensating the energy losses in order to stabilize the soliton.

Finally, for the momentum

$$P = \frac{i}{2}\int_{-\infty}^{+\infty} dx(\bar{\Psi}_x\gamma^0\Psi - \bar{\Psi}\gamma^0\Psi_x) \tag{29}$$

one obtains

$$\frac{dP}{dt} = -2\rho P + \int_{-\infty}^{+\infty} dx(f\bar{\Psi}_x\Psi^\star + f^\star\bar{\Psi}^\star\Psi_x). \tag{30}$$

The source terms are given on the rhs of the continuity Eqs. (25), (28), and (30). Obviously, for $f = 0$ and $\rho = 0$, all these terms are zero and the charge, the energy, and the momentum become conserved magnitudes. In the case of the exact stationary solutions of Eq. (4) found in Sec. II, the relationships (16), (17), and (20) cause the source terms to cancel out in each continuity equation and, consequently, the charge, the energy, and the momentum are also preserved. Explicit expressions for these magnitudes can be obtained by inserting the

stationary solutions (23) into the definitions (24), (26), and (29) and then integrating. This procedure yields

$$Q_\pm = \int_{-\infty}^{+\infty} dx \left[A_\pm^2(x) + B_\pm^2(x)\right] = \frac{2\sqrt{m^2-\omega_\pm^2}}{g^2\omega_\pm} \tag{31}$$

and

$$\begin{aligned} E_\pm &= \int_{-\infty}^{+\infty} dx \left\{m\left[A_\pm^2(x) - B_\pm^2(x)\right]\right\} \pm \sqrt{r^2-\rho^2}Q_\pm \\ &= M_\pm \pm \sqrt{r^2-\rho^2}Q_\pm, \end{aligned} \tag{32}$$

where $M_\pm = \frac{4m}{g^2}\,\text{arctanh}\left(\sqrt{\frac{m-\omega_\pm}{m+\omega_\pm}}\right)$. The momentum is null $P_\pm = 0$, because, curiously, even the momentum density is zero.

From these expressions, a counterintuitive fact can be deduced; namely, that in the stationary solution $\Psi_-(x,t)$, the dissipation increases the values of the charge and the energy. This behavior can be appreciated in Fig. 1, where the contour plots of the charge, Q_-, and the energy, E_-, are shown as functions of the dissipation coefficient ρ and of the driving frequency ν, for fixed values of r, m, and g. The arrows point out that, for constant ν, the larger ρ becomes, the larger the charge and the energy also become. This feature is an indication of the unstable nature of this solution.

IV. STABILITY OF THE EXACT STATIONARY SOLUTIONS

In order to study the stability of the exact stationary solutions (23), let us consider initial conditions which deviate a little from the exact solutions. Let us also assume that, specifically, these small deviations affect the values of the parameter $\omega_\pm$ and the phase $\Theta_\pm$ of the exact solutions in such a way that an approximated solution of Eq. (4) is captured by the ansatz

$$\Psi_{1a}(x,t) = e^{-i\left[\frac{\nu}{2}t+\phi(t)\right]}\frac{\sqrt{2}\beta(t)}{g}\frac{\sqrt{m+\omega(t)}\cosh\left[\beta(t)x\right]}{m+\omega(t)\cosh[2\beta(t)x]}, \tag{33}$$

$$\Psi_{2a}(x,t) = ie^{-i\left[\frac{\nu}{2}t+\phi(t)\right]}\frac{\sqrt{2}\beta(t)}{g}\frac{\sqrt{m-\omega(t)}\sinh\left[\beta(t)x\right]}{m+\omega(t)\cosh[2\beta(t)x]}, \tag{34}$$

where the phase $\phi(t)$ and the frequency $\omega(t)$ now deviate from their constant values $\Theta_\pm/2$ and $\omega_\pm$, respectively, and become functions of time. Small deviations of the frequency ν are implicitly taken into account in the time-dependent phase $\phi(t)$. Additionally, $\beta(t) = \sqrt{m^2-\omega^2(t)}$ also depends on time. This is a standard procedure in the soliton theory when perturbations are introduced,[24,35,41–43] but here only two collective variables have been employed instead of the five coordinates needed to describe solitons of the NLD equation with an inhomogeneous parametric force. By inserting (33)–(34) into (7) and (8) and integrating over x, the Lagrangian and the dissipation functions are, respectively, obtained as

$$L_a[\phi(t),\omega(t),\dot\phi(t)] = Q_a[\omega(t)]\left(\dot\phi(t)+\frac{\nu}{2}\right) - E_a[\phi(t),\omega(t)], \tag{35}$$

$$F_a[\omega(t),\dot\phi(t)] = -2\rho\left(\dot\phi(t)+\frac{\nu}{2}\right)Q_a[\omega(t)], \tag{36}$$

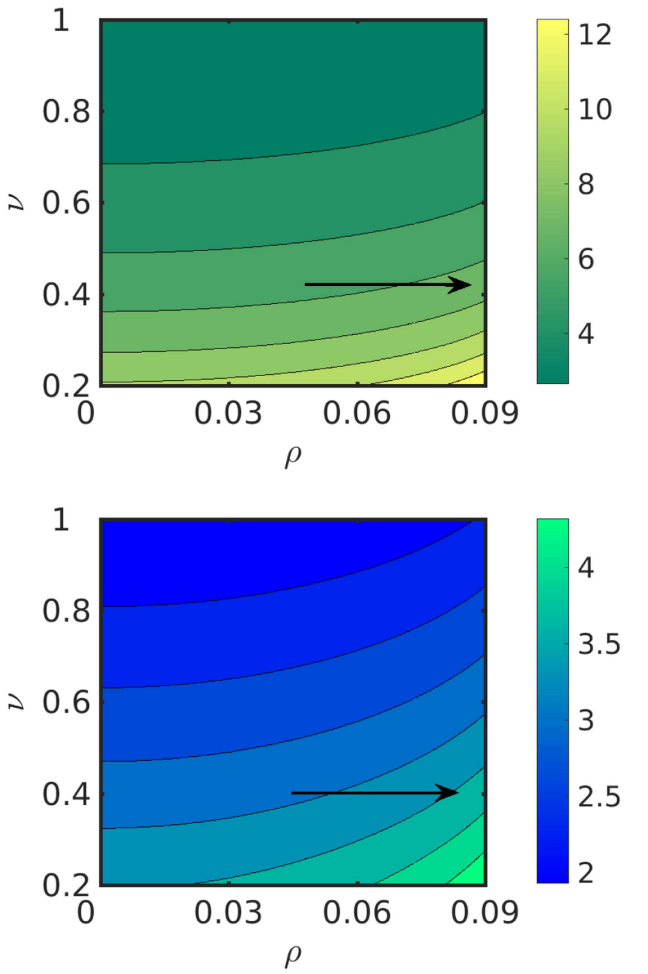

FIG. 1. Contour plots of the charge (upper panel) and the energy (lower panel) vs ρ and ν. The arrows show that for fixed frequency, the charge and the energy increase with ρ. Other parameters: $m = 1$, $g = 1$, $r = 0.1$, and $\Theta_- = \pi - \arcsin(\rho/r)$.

where the dot indicates the derivative with respect to time, and where

$$Q_a[\omega(t)] = \frac{2\beta(t)}{g^2\omega(t)}, \tag{37}$$

$$\begin{aligned} E_a[\phi(t),\omega(t)] = {} & \frac{4\,m}{g^2}\,\text{arctanh}\left(\sqrt{\frac{m-\omega(t)}{m+\omega(t)}}\right) \\ & + r\cos[2\,\phi(t)]Q_a[\omega(t)] \end{aligned} \tag{38}$$

are the charge and the energy of the approximate solution, respectively.

From the Lagrange equations corresponding to (35) and (36), the following autonomous system of equations for the phase $\phi(t)$ and

the frequency $\omega(t)$ is easily derived:

$$\dot{\phi}(t) = \omega(t) - \frac{\nu}{2} + r\cos[2\phi(t)], \tag{39}$$

$$\dot{\omega}(t) = -\frac{2\omega(t)\beta^2(t)}{m^2}\{r\sin[2\phi(t)] - \rho\}. \tag{40}$$

These equations are completed with the initial conditions $\omega(0)$ and $\phi(0)$. A more complex ansatz, including a momentum and the soliton center-of-mass, provides no significant additional information and also leads to Eqs. (39) and (40). Notice that this dynamical system does not depend explicitly on time thanks to separate $\nu t/2$ and $\phi(t)$ expressly in the ansatz (33) and (34). In this way, the dynamics of the parametrically driven and damped NLD equation (4) with infinite degrees of freedom has been reduced to the study of two nonlinear ordinary differential equations, whose analysis is expected to provide a good insight into the evolution of the system.

Firstly, by setting $\dot{\phi}(t) = 0$ and $\dot{\omega}(t) = 0$ in Eqs. (39) and (40), and by solving the resulting algebraic equations, the following equilibrium points are obtained

$$\phi_s = \frac{\pi}{4}(1-s) + \frac{s}{2}\arcsin\left(\frac{\rho}{r}\right), \tag{41}$$

$$\omega_s = \frac{\nu}{2} - s\sqrt{r^2-\rho^2}, \tag{42}$$

where s can take the values $+1$ or -1. Clearly, these equilibrium points correspond to the phases, $\Theta_\pm/2$, and the frequencies, $\omega_\pm$, of the exact stationary solutions found in Sec. II.

In order to study the stability of the fixed points, we linearize Eqs. (39) and (40) around these points

$$\begin{bmatrix}\delta\dot{\phi}\\ \delta\dot{\omega}\end{bmatrix} = \begin{bmatrix}-2\rho & 1\\ -s\sigma_s^2 & 0\end{bmatrix}\begin{bmatrix}\delta\phi\\ \delta\omega\end{bmatrix}, \tag{43}$$

where $\delta\phi(t)$ and $\delta\omega(t)$ represent small deviations from the equilibrium values ϕ_s and ω_s, respectively, and where

$$\sigma_s^2 = \frac{4\omega_s(m^2-\omega_s^2)\sqrt{r^2-\rho^2}}{m^2} > 0 \tag{44}$$

is a real positive parameter. The eigenvalues of the matrix

$$\mathbf{A} = \begin{bmatrix}-2\rho & 1\\ -s\sigma_s^2 & 0\end{bmatrix} \tag{45}$$

associated to the linear problem are

$$\lambda_{1,2} = -\rho \pm \sqrt{\rho^2 - s\sigma_s^2}. \tag{46}$$

For $s=-1$, the two eigenvalues are real and have different signs. Hence, the equilibrium point (ω_{-1},ϕ_{-1}) is always an unstable saddle point. However, for $s=+1$, there are three possibilities. If $\rho=0$, then the eigenvalues of $\mathbf{A}$ are imaginary and (ϕ_{+1},ω_{+1}) is a center (see red line in Fig. 2). Nevertheless, if $0<\rho<\sigma_{+1}$, then the two eigenvalues are complex conjugates with a negative real part and the equilibrium point (ϕ_{+1},ω_{+1}) is an stable focus (cyan region in Fig. 2 for $\nu=1$). When $\rho\geq\sigma_{+1}$, then the two eigenvalues become negative real values and (ϕ_{+1},ω_{+1}) transforms into a stable node (green region).

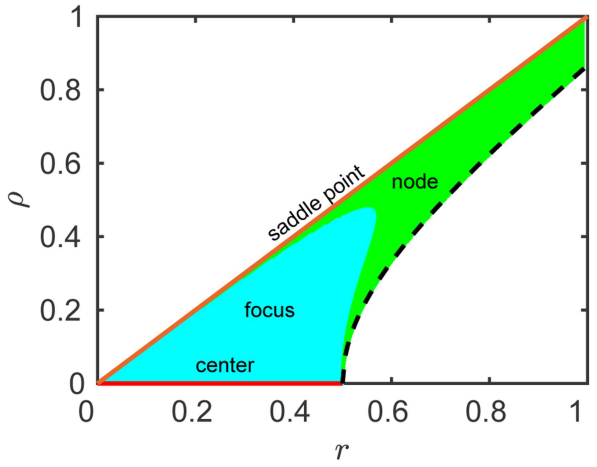

FIG. 2. Stability diagram for $r\in[0,1]$ and $\rho_{min}\leq\rho\leq r$. The fixed point (ϕ_+,ω_+) can be a stable center (red line), a stable focus (cyan region), a stable node (green region) or an unstable saddle point (orange line $\rho=r$). The dashed line represents the minimum possible value of ρ: $\rho_{min}=\sqrt{\max(0,r^2-[1-\nu/2]^2)}$. Other parameters: $m=1$, $g=1$, $\nu=1$.

Finally, it is necessary to consider the limiting case $\rho\to r$, in which the two equilibrium points collide, resulting in only one fixed point at $(\pi/4,\nu/2)$. These coordinates are simply the mean value between the two fixed points, (ϕ_{-1},ω_{-1}) and (ϕ_{+1},ω_{+1}), and correspond to the orange line in Fig. 2. In this case, the parameter $\sigma_s=0$ and, consequently, the linear analysis provides no information regarding its stability. However, by integrating numerically (39) and (40), it can be easily verified that it is an unstable equilibrium point.

The above linear stability analysis is illustrated in Fig. 3 with two phase portraits on the plane (ϕ,ω). The phase portrait displayed in the upper panel corresponds to the nondissipative case ($\rho=0$), while for the lower panel, $\rho=0.05$. In both panels, the solid circles represent the equilibrium points, the blue arrowed lines are stream plots of the vector field $(\dot{\phi},\dot{\omega})$, and the thick colored lines are depictive trajectories generated from specific initial conditions.

In the top panel of Fig. 3, the center at $(\phi_{+1},\omega_{+1})=(0,0.4)$ represents the stable solution $\Psi_+(x,t)$. In its neighborhood, the system trajectories are closed loops. The red small periodic orbit corresponds to the initial condition $(0,0.5)$, while the green large periodic orbit is obtained using a perturbation $\delta\phi=-0.05$ around the solid point at $(\phi_{-1},\omega_{-1})=(\pi/2,0.6)$, which represents the unstable solution $\Psi_-(x,t)$. At a sufficient distance from the center, one finds trajectories whose phases increase monotonously like, for instance, the upper orange line that passes through $(\phi_{-1},\omega_{-1}+0.1)$. Analytical expression for these orbits can be derived from a conservation law. Indeed, by inserting the ansatz (33) and (34) into the energy balance (28) it is obtained

$$\frac{dE_a}{dt} = F_a + \frac{\nu}{2}\frac{dQ_a}{dt}. \tag{47}$$

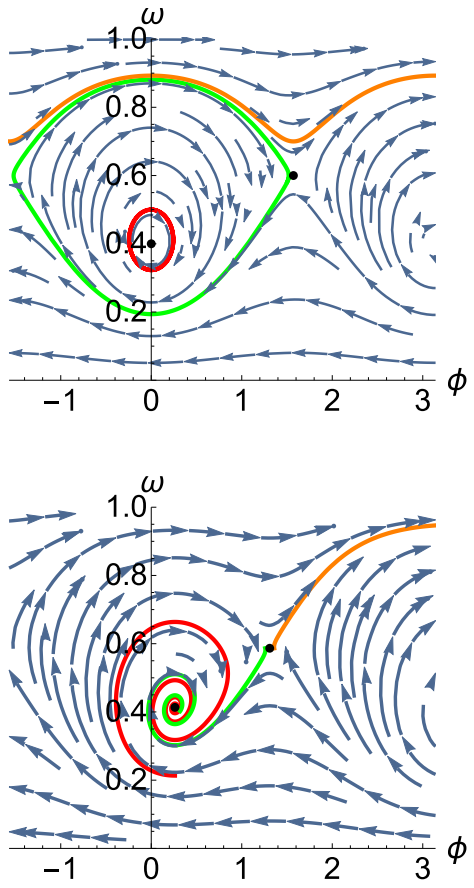

FIG. 3. Phase portraits of the autonomous Eqs. (39) and (40) for the nondissipative case $\rho = 0$ (upper panel) and for the dissipative case $\rho = 0.05$ (lower panel). The solid circles represent the equilibrium points, the blue arrowed lines are stream plots of the vector field $(\dot{\phi}, \dot{\omega})$, and the thick colored lines are trajectories generated from specific initial conditions (see text for details). Other parameters: $m = 1$, $g = 1$, $\nu = 1$, $r = 0.1$.

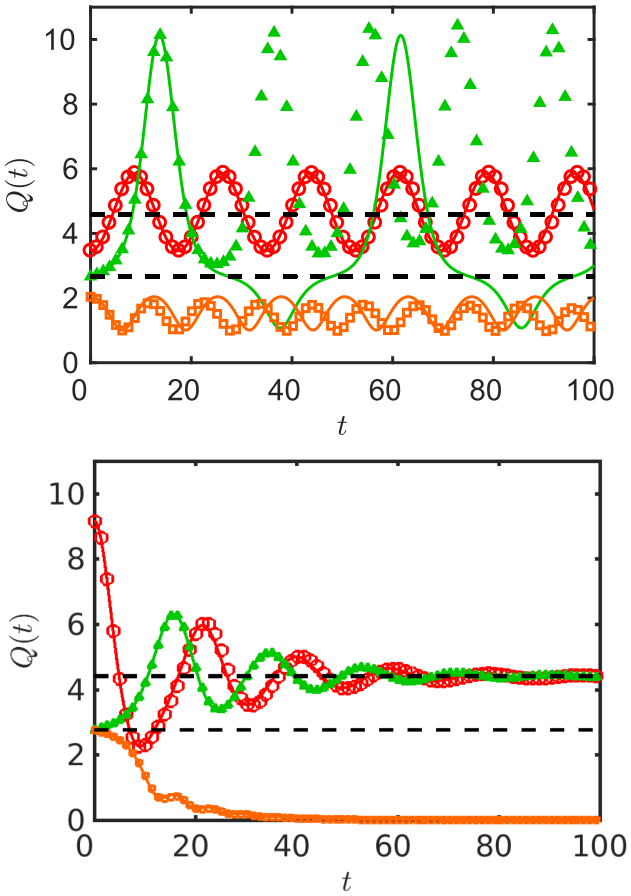

FIG. 4. Evolution of the soliton charge in time for the set of initial conditions corresponding to the colored trajectories plotted in Fig. 3. The symbols represent simulation results of the parametrically driven, damped NLD Eq. (4), while the solid lines are the approximation (37). The dashed lines correspond to the charges of the stable (upper line) and unstable (lower line) stationary solutions. Upper panel: nondissipative case ($\rho = 0$). Lower panel: dissipative case with $\rho = 0.05$. Other parameters: $m = 1$, $g = 1$, $\nu = 1$, $r = 0.1$.

In the nondissipative case, $F_a = 0$ and, therefore, it fulfils $\frac{d}{dt}\left(E_a - \frac{\nu}{2}Q_a\right) = 0$. Thus, the orbits on the phase portrait (upper panel of Fig. 3) correspond to different values of the conserved quantity $E_a - \frac{\nu}{2}Q_a$, that is, the equation of the orbits is

$$\frac{4m}{g^2}\,\mathrm{arctanh}\left(\sqrt{\frac{m-\omega}{m+\omega}}\right) + \left[r\cos(2\phi) - \frac{\nu}{2}\right]\frac{2\sqrt{m^2-\omega^2}}{g^2\omega} = C, \tag{48}$$

where the constant of integration C is determined by the initial conditions.

In the lower panel of Fig. 3, the stable solution $\Psi_+(x,t)$ is now a focus represented by a black solid point at $(\phi_{+1}, \omega_{+1}) = (\pi/12, 0.41)$. In its neighborhood, the system trajectories are spirals. The red spiral arises from $(\phi_{+1}, \omega_{+1} - 0.2)$ while the green spiral comes from the vicinity of the unstable fixed point at $(\phi_{-1}, \omega_{-1}) = (5\pi/12, 0.59)$, using a perturbation $\delta\phi = -0.05$. If the sign of this last perturbation is changed, the orange trajectory on the upper right-hand region is obtained.

In order to verify the predictions of the stability analysis, the parametrically driven, damped NLD Eq. (4) has been numerically integrated, by taking the functions (33)–(34), evaluated at $t = 0$, as the initial condition. The same set of values $(\phi(0), \omega(0))$ employed to generate the colored trajectories of Fig. 3 has been considered. For this set of initial conditions, the time evolution of the charge $Q(t)$ (symbols) is compared in Fig. 4 with the approximate expression (37) plotted with solid lines. The dashed horizontal lines are the charges of the stable (upper line) and unstable (lower line) stationary states. Again, the nondissipative case is displayed in the upper panel. The circles correspond to the small red orbit shown in the upper panel of Fig. 3 and the triangles to the large green orbit arising in the vicinity

of the unstable equilibrium point. The oscillations represented by the squares correspond to the upper orange trajectory in the upper panel of Fig. 3. Note that for short times, there is an excellent agreement between the exact numerical results and the approximation (37). For longer times, the small red orbit around the center is well captured by the approximation, while significant deviations appear for the large green orbit. These deviations are due to the fact that the green orbit is located in a very sensitive region, very close to the separatrix of the attraction domain of the center.

The case $\rho = 0.05$ is shown in the lower panel of Fig. 4. Here, the circles and triangles correspond to the spirals that converge towards the stable equilibrium point. The upper right-hand orange trajectory in the lower panel of Fig. 3 corresponds to the squares, whose decay to zero indicates that the initial soliton is destroyed. In this case, the agreement between numerical results and the approximation (37) is excellent for all trajectories. Similar results have been obtained when the equilibrium points are nodes. Therefore, the numerical simulations of the NLD Eq. (4) confirm the predictions regarding the stability of the stationary solutions based on the study of the autonomous ordinary differential equations (39) and (40).

It is worth mentioning that the numerical simulations of the NLD equation have been performed by using a Runge-Kutta-Verner fifth-order algorithm with a variable time step, and a spectral method for computing the spatial derivatives.[44] Periodic boundary conditions have also been employed. The system has been discretized by taking constant spatial intervals $\Delta x = 0.02$, and a number of points $N = 3200$ so that its length is $L = N\Delta x = 64$.

V. CONCLUSIONS

The parametrically driven, damped Nonlinear Dirac equation has been investigated. In particular, two exact stationary soliton solutions, $\Psi_+(x,t)$ and $\Psi_-(x,t)$, have been found when the parametric pumping is a complex time-periodic force.

In order to obtain these solutions, three conditions have to be fulfilled, namely, the dissipation coefficient must be less than or equal to the amplitude of the force, the frequency of the stationary solutions has to be locked to half of the frequency of the parametric force, and, finally, their phases are determined by the dissipation coefficient and the amplitude of the force through the relations (16) and (17). Under these conditions, we demonstrate that the damped parametrically driven nonlinear Dirac equation reduces to a system of two well-known nonlinear equations. As a result, the functional form of the solutions is similar to that of the NLD equation without perturbations. Additionally, explicit expressions for the charge, the energy, and the momentum of these solutions have also been provided.

A significant part of our work has been focused on the analysis of the stability of these solutions. By means of a variational method and by employing an ansatz with only two collective variables, the dynamics of the solitons have been studied for initial conditions that slightly deviate from the exact solutions. In this way, the infinite degree of freedom problem was reduced to an autonomous dynamical system with only two degrees of freedom. This last system possesses two fixed points which correspond to the two exact stationary solutions. A linear stability analysis predicts that $\Psi_+(x,t)$ is stable, whereas $\Psi_-(x,t)$ is unstable. Phase portraits for both the dissipative and the nondissipative regime have been provided. Specifically, the fixed point related with $\Psi_+(x,t)$ is a center in the nondissipative regime. For low damping it is a focus, and it becomes a node for a sufficiently large dissipation. The second fixed point corresponding to $\Psi_-(x,t)$ is always an unstable saddle point. All these predictions have been confirmed by numerical simulations of the damped, parametrically driven NLD Eq. (4).

Therefore, a time-periodic parametric driving can be used to stabilize the damped NLD soliton. Precise relationships among the damping coefficient, the amplitude, and the frequency of the ac parametric force lead to a balance between energy gains and losses that stabilizes the soliton $\Psi_+(x,t)$. Remarkably, this is not possible to achieve in the damped NLD equation with nonhomogeneous parametric forces, where the introduction of dissipation always leads to soliton destruction. This finding could be valuable in the context of the stabilization of two-dimensional nonlinear excitations governed by the nonlinear Dirac equation, such as relativistic vortices in Bose-Einstein condensates[45] or solitons in the honeycomb lattice.[46] Another interesting extension of our work involves the search of exact travelling soliton solutions in the damped parametrically driven NLD equation. Both topics deserve further theoretical investigation.

ACKNOWLEDGMENTS

We acknowledge financial support from the Junta de Andalucía, from the Ministerio de Economía y Competitividad of Spain through FIS2017-89349-P (N.R.Q.) and from the Ministerio de Ciencia, Innovación y Universidades of Spain through PGC2018-093998-B-I00 (B.S.R.). N.R.Q. also acknowledges financial support from the Alexander von Humboldt Foundation and the hospitality of the Physikalisches Institut at the University of Bayreuth (Germany) during the development of this work.

REFERENCES

[1] V. A. Brazhnyi, V. V. Konotop, S. Coulibaly, and M. Taki, "Field patterns in periodically modulated optical parametric amplifiers and oscillators," Chaos **17**, 037111 (2007).
[2] A. Vinante and P. Falferi, "Feedback-enhanced parametric squeezing of mechanical motion," Phys. Rev. Lett. **111**, 207203 (2013).
[3] M. J. Seitner, M. Abdi, A. Ridolfo, M. J. Hartmann, and E. M. Weig, "Parametric oscillation, frequency mixing, and injection locking of strongly coupled nanomechanical resonator modes," Phys. Rev. Lett. **118**, 254301 (2017).
[4] I. V. Barashenkov, *The Continuing Story of the Wobbling Kink, Chapter in A Dynamical Perspective on the ϕ^4 Model* (Springer, 2019).
[5] P. Engels, C. Atherton, and M. A. Hoefer, "Observation of Faraday waves in a Bose-Einstein condensate," Phys. Rev. Lett. **98**, 095301 (2007).
[6] K. Ohlin and K. F. Berggren, "Patterns beyond Faraday waves: Observation of parametric crossover from Faraday instabilities to the formation of vortex lattices in open dual fluid strata," Eur. J. Phys. **37**, 045803 (2016).
[7] A. Garcimartín, D. Maza, J. L. Ilquimiche, and I. Zuriguel, "Convective motion in a vibrated granular layer," Phys. Rev. E **65**, 031303 (2002).
[8] E. Zamora-Sillero, N. R. Quintero, and F. G. Mertens, "Ratchet effect in a damped sine-Gordon system with additive and parametric ac driving forces," Phys. Rev. E **74**, 046607 (2006).
[9] X. Noblin, R. Kofman, and F. Celestini, "Ratchetlike motion of a shaken drop," Phys. Rev. Lett. **102**, 194504 (2009).
[10] N. Casic, N. Quintero, R. Alvarez-Nodarse, F. G. Mertens, L. Jibuti, W. Zimmermann, and T. M. Fischer, "Propulsion efficiency of a dynamic self-assembled helical ribbon," Phys. Rev. Lett. **110**, 168302 (2013).
[11] R. Meucci, W. Gadomski, M. Ciofini, and F. T. Arecchi, "Experimental control of chaos by means of weak parametric perturbations," Phys. Rev. E **49**, R2528 (1994).

[12]Y. S. Kivshar and K. H. Spatschek, "Nonlinear dynamics and solitons in the presence of rapidly varying periodic perturbations," Chaos Solitons Fractals **5**, 2551 (1995).
[13]I. V. Barashenkov, N. V. Alexeeva, and E. V. Zemlyanaya, "Two- and three-dimensional oscillons in nonlinear Faraday resonance," Phys. Rev. Lett. **89**, 104101 (2002).
[14]N. R. Quintero, A. Sánchez, and F. G. Mertens, "Anomalies of ac driven solitary waves with internal modes: Nonparametric resonances induced by parametric forces," Phys. Rev. E **64**, 046601 (2001).
[15]M. M. Bogdan, A. M. Kosevich, and I. V. Manzhos, "Stabilization of a magnetic soliton (bion) as a result of parametric excitation of one-dimensional ferromagnet," Fiz. Nizk. Temp. **11**, 991 (1985).
[16]I. V. Barashenkov, M. M. Bogdan, and V. I. Korobov, "Stability diagram of the phase-locked solitons in the parametrically driven, damped nonlinear Schrödinger equation," Europhys. Lett. **15**, 113 (1991).
[17]L. D. Landau and E. M. Lifshitz, *Mechanics (Course of Theoretical Physics)*, 3rd ed. (Pergamon Press, Oxford, 1976), Vol. 1.
[18]A. H. Nayfeh and D. T. Mook, *Nonlinear Oscillations* (Wiley, 1995).
[19]S. Sonar, V. Fedoseev, M. J. Weaver, F. Luna, E. Vlieg, H. van der Meer, and D. B. W. Löffler, "Strong thermomechanical squeezing in a far-detuned membrane-in-the-middle system," Phys. Rev. A **98**, 013804 (2018).
[20]A. Sánchez, A. R. Bishop, and F. Domínguez-Adame, "Kink stability, propagation, and length-scale competition in the periodically modulated sine-Gordon equation," Phys. Rev. E **49**, 4603 (1994).
[21]R. Scharf and A. R. Bishop, "Length-scale competition for the one-dimensional nonlinear Schrödinger equation with spatially periodic potentials," Phys. Rev. E **47**, 1375 (1993).
[22]J. J. García-Ripoll, V. M. Pérez-García, and P. Torres, "Extended parametric resonances in nonlinear Schrödinger systems," Phys. Rev. Lett. **83**, 1715 (1999).
[23]I. V. Barashenkov, E. V. Zemlyanaya, and M. Bär, "Traveling solitons in the parametrically driven nonlinear Schrödinger equation," Phys. Rev. E **64**, 016603 (2001).
[24]S. Cuenda and A. Sánchez, "Length scale competition in nonlinear Klein-Gordon models: A collective coordinate approach," Chaos **15**, 023502 (2005).
[25]V. M. Pérez-García, P. J. Torres, and V. V. Konotop, "Similarity transformations for nonlinear Schrödinger equations with time-dependent coefficients," Physica D **221**, 31 (2006).
[26]L. Dinis and N. R. Quintero, "Nonsinusoidal current and current reversals in a gating ratchet," Phys. Rev. E **91**, 032920 (2015).
[27]A. Sánchez and A. R. Bishop, "Collective coordinates and length-scale competition in spatially inhomogeneous soliton-bearing equations," SIAM Rev. **40**, 579 (1998).
[28]O. F. Oxtoby and I. V. Barashenkov, "Resonantly driven wobbling kinks," Phys. Rev. E **80**, 026609 (2009).
[29]I. V. Barashenkov and O. F. Oxtoby, "Wobbling kinks in ϕ^4 theory," Phys. Rev. E **80**, 026608 (2009).
[30]S. Cuenda, N. R. Quintero, and A. Sánchez, "Sine-Gordon wobbles through Bäcklund transformations," Discrete Continuous Dynamical Syst. S **4**, 1047 (2011).
[31]Y. S. Kivshar, N. Grønbech-Jensen, and M. R. Samuelsen, "π kinks in a parametrically driven sine-Gordon chain," Phys. Rev. B **45**, 7789 (1992).
[32]S. Y. Lee, T. K. Kuo, and A. Gavrielides, "Exact localized solutions of two-dimensional field theories of massive fermions with Fermi interactions," Phys. Rev. D **12**, 2249 (1975).
[33]L. H. Haddad and L. D. Carr, "The nonlinear Dirac equation in Bose-Einstein condensates: Foundation and symmetries," Physica D **238**, 1413 (2009).
[34]T. X. Tran, S. Longhi, and F. Biancalana, "Optical analogue of relativistic Dirac solitons in binary waveguide arrays," Ann. Phys. (N. Y) **340**, 179 (2014).
[35]F. G. Mertens, N. R. Quintero, F. Cooper, A. Khare, and A. Saxena, "Nonlinear Dirac equation solitary waves in external fields," Phys. Rev. E **86**, 046602 (2012).
[36]S. Shao and H. Tang, "Interaction for the solitary waves of a nonlinear Dirac model," Phys. Lett. A **345**, 119 (2005).
[37]N. R. Quintero, S. Shao, R. Alvarez-Nodarse, and F. G. Mertens, "Externally driven nonlinear Dirac equation revisited: Theory and simulations," J. Phys. A Math. Theor. **52**, 155401 (2019).
[38]N. R. Quintero, B. Sánchez-Rey, F. Cooper, and F. G. Mertens, "Length-scale competition in the parametrically driven nonlinear Dirac equation with a spatially periodic force," J. Phys. A Math. Theor. **52**, 285201 (2019).
[39]A. Alvarez and B. Carreras, "Interaction dynamics for the solitary waves of a nonlinear Dirac model," Phys. Lett. A **86**, 327 (1981).
[40]J. Ruiz-Rivas, G. J. de Valcárcel, and C. Navarrete-Benlloch, "Active locking and entanglement in type II optical parametric oscillators," New J. Phys. **20**, 023004 (2018).
[41]Y. Nogami and F. M. Toyama, "Transparent potential for the one-dimensional Dirac equation," Phys. Rev. A **45**, 5258 (1992).
[42]F. G. Mertens, F. Cooper, N. R. Quintero, S. Shao, A. Khare, and A. Saxena, "Solitary waves in the nonlinear Dirac equation in the presence of external driving forces," J. Phys. A Math. Theor. **49**, 065402 (2016).
[43]Y. Zolotaryuk and M. M. Osmanov, "Directed motion of domain walls in biaxial ferromagnets under the influence of periodic external magnetic fields," Eur. Phys. J. B **79**, 257 (2011).
[44]J. Cuevas-Maraver, P. Kevrekidis, A. Saxena, F. Cooper, and F. Mertens, *Solitary Waves in the Nonlinear Dirac Equation at the Continuum Limit: Stability and Dynamics* (Nova Sciences, New York, 2015).
[45]L. H. Haddad, K. M. O'Hara, and L. D. Carr, "Nonlinear Dirac equation in Bose-Einstein condensates: Preparation and stability of relativistic vortices," Phys. Rev. A **91**, 043609 (2015).
[46]E. Arévalo and L. Morales-Molina, "Nonlinear excitations in the honeycomb lattice: Beyond the high-symmetry points of the band structure," Phys. Rev. A **93**, 053816 (2016).